

Applicability of Euler-Lagrange coupling multiphase-flow model to bed-load transport under high bottom shear

Possibilité d'application d'un modèle multiphasique Euler-Lagrangien au transport par charriage dans un écoulement à forte contrainte de cisaillement

ABBAS YEGANEH (BAKHTIARY), *Post-doctoral Research Fellow, Department of Civil Engineering, Graduate School of Engineering, Kyoto University, Yoshida Hon-machi, Sakyo-ku, Kyoto, 606-8501, Japan, E-mail: k52689@sakura.kudpc.kyoto-u.ac.jp*

HITOSHI GOTOH, *Associate Professor, Department of Civil Engineering, Graduate School of Engineering, Kyoto University, E-mail: gotoh@coast.kuciv.kyoto-u.ac.jp*

TETSUO SAKAI, *Professor, Department of Civil Engineering, Graduate School of Engineering, Kyoto University, E-mail: sakai@coast.kuciv.kyoto-u.ac.jp*

ABSTRACT

Bed-load transport at high shear stress is numerically simulated with the aid of the two-phase flow model, in which Euler-Lagrange coupling of the governing equations of the fluid and sediment phases are implemented. Fluid phase is described by the vertically two-dimensional $k-\varepsilon$ turbulence model in unidirectional flow condition, while the sediment motion is expressed by the numerical tracing of the saltating particles. The fluid/particle interaction, as the main interaction mechanism, is explicitly introduced into the governing equations in the present model. The characteristics of the mean-flow velocity profile of the saltation dominant flow, namely two-layer profile, is reproduced well with the present model. Experimental results show the existence of the three-layer type velocity profile under the high bottom shear, while the present model cannot reproduce such characteristics. The limitation of the assumption in the present model by neglecting the existence of the interparticle collision will be discussed on the basis of the results of the simulation.

RÉSUMÉ

Le transport solide par charriage sous un fort cisaillement est simulé numériquement à l'aide d'un modèle diphasique Euler-Lagrangien couplé. La phase fluide est décrite par un modèle de turbulence $k-\varepsilon$, 2D vertical dans un écoulement unidirectionnel, tandis que le mouvement de la phase solide sédimentaire est exprimé par le suivi lagrangien des particules en saltation.

L'interaction fluide/particule, considérée comme prépondérante, est introduite de façon explicite dans les équations du modèle. Les caractéristiques des profils de vitesse moyenne pour des écoulements où la saltation est dominante, à savoir les profils à deux couches, sont bien reproduites par le présent modèle. Les résultats expérimentaux montrent l'existence d'un profil de vitesse comportant trois couches lorsque le cisaillement est très important, ce que le modèle ne peut reproduire. Les limites de l'hypothèse consistant à négliger les collisions entre les particules sont discutées à partir des résultats de la simulation.

1 Introduction

Accuracy of the modeling of bed-load transport depends on how well the hydrodynamics is described. As far as the bottom shear stress is low, this hydrodynamics can be expressed with the interaction mechanism of fluid flow and sediment particles, namely the fluid/particle interaction. But, high bottom shear stress induces the intense sediment transport especially near the bottom, then the hyper-concentrated layer of moving sediments occurs. In this layer, the frequent interparticle collision brings another predominant interaction mechanism to the bed-load hydrodynamics, the so-called particle/particle interaction.

A two-phase flow model provides a very powerful simulation tool to describe the bed-load hydrodynamics. In the two-phase flow model, the governing equations of fluid phase are generally described in Eulerian form; whereas, the governing equations of the sediment phase can be written in either Eulerian or Lagrangian form. Furthermore, by coupling the governing equations of both phases, a system of the Eulerian equations or Euler-Lagrange coupled ones is obtained to analyze the sediment-laden flow.

In the Euler-Euler coupling model, the sediment phase is treated as a continuum, which follows to the different kind of the con-

stitutive law from that of the clear-water. The main deficiency of this kind of model is that the probabilistic characteristics of sediment motion is ignored. Kobayashi and Seo (1985); Bakker and Kesteren (1986); and Asano (1990) should be mentioned among the studies devoted to the Euler-Euler coupling model.

The probabilistic character of sediment motion can be described well with the aid of a Lagrangian model. In this type of models, the following key points should be included: (i) the random motion of the sediment particles with the irregular collision and repulsion at the bed; (ii) the interphase momentum exchange; and (iii) the momentum transfer during the collision and repulsion.

So far, some studies have been conducted on the simulation of bed-load transport by using a stochastic model of successive saltating particles in the unidirectional flow. Most of them, however, were constructed based on the clear-water assumption which we term as the one-way model. Wiberg and Smith (1989) performed a numerical simulation based on the Euler-Lagrange two-way model by coupling the irregular successive saltation model with the mixing length model. Later, Gotoh, Tsujimoto and Nakagawa (1994) proposed the Euler-Lagrange two-way model by coupling the irregular successive saltation model with

Revision received August, 1999. Open for discussion till April 30, 2001.

the k - ε turbulence model. In the model of Gotoh et al., the fluid/particle interaction was described with the aid of the Particle-Source-In (PSI) cell method, without considering the effects of turbulence on the trajectory of saltating particle.

Although, a few numerical studies on the bed-load transport have been conducted with the Euler-Lagrange coupling, to the best knowledge of the authors, even very little information is available on the modeling of bed-load at high bottom shear stresses. In this study, we apply the coupling of the irregular successive saltation model with the k - ε turbulence model to the sediment-laden flow under various level of bottom shear stress, to investigate the applicability of such a framework to the sediment-laden flow at high bottom shear.

2 Simulation model

2.1 Model of fluid phase

The governing equations of the fluid phase is implemented in the vertically two-dimensional coordinates as follows:

$$\frac{\partial U}{\partial x} + \frac{\partial V}{\partial y} = 0 \quad (1)$$

$$U \frac{\partial U}{\partial x} + V \frac{\partial U}{\partial y} = g \sin \theta - \frac{1}{\rho} \frac{\partial P}{\partial x} + \frac{\partial}{\partial x} \left(2\Gamma \frac{\partial U}{\partial x} \right) + \frac{\partial}{\partial y} \left\{ \Gamma \left(\frac{\partial U}{\partial y} + \frac{\partial V}{\partial x} \right) \right\} + \frac{F_{dx}}{\rho(1-C)} \quad (2)$$

$$U \frac{\partial V}{\partial x} + V \frac{\partial V}{\partial y} = g \cos \theta - \frac{1}{\rho} \frac{\partial P}{\partial y} + \frac{\partial}{\partial x} \left\{ \Gamma \left(\frac{\partial U}{\partial y} + \frac{\partial V}{\partial x} \right) \right\} + \frac{\partial}{\partial y} \left(2\Gamma \frac{\partial V}{\partial y} \right) + \frac{F_{dy}}{\rho(1-C)} \quad (3)$$

$$U \frac{\partial k}{\partial x} + V \frac{\partial k}{\partial y} = \frac{\partial}{\partial x} \left\{ \left(v + \frac{v_t}{\sigma_k} \right) \frac{\partial k}{\partial x} \right\} + \frac{\partial}{\partial y} \left\{ \left(v + \frac{v_t}{\sigma_k} \right) \frac{\partial k}{\partial y} \right\} + P_r + G - \varepsilon + \frac{\overline{u f_{dx}} + \overline{v f_{dy}}}{\rho(1-C)} \quad (4)$$

$$U \frac{\partial \varepsilon}{\partial x} + V \frac{\partial \varepsilon}{\partial y} = \frac{\partial}{\partial x} \left\{ \left(v + \frac{v_t}{\sigma_\varepsilon} \right) \frac{\partial \varepsilon}{\partial x} \right\} + \frac{\partial}{\partial y} \left\{ \left(v + \frac{v_t}{\sigma_\varepsilon} \right) \frac{\partial \varepsilon}{\partial y} \right\} + \frac{\varepsilon}{k} (C_{1\varepsilon} P_r + C_{2\varepsilon} G - C_{3\varepsilon} \varepsilon) + \frac{\varepsilon}{k} \left(\frac{\overline{u f_{dx}} + \overline{v f_{dy}}}{\rho(1-C)} \right) \quad (5)$$

$$P_r = v_t \left[2 \left\{ \left(\frac{\partial U}{\partial x} \right)^2 + \left(\frac{\partial V}{\partial y} \right)^2 + \left(\frac{\partial U}{\partial x} + \frac{\partial V}{\partial y} \right)^2 \right\} \right] \quad (6)$$

$$G = \frac{\sigma - \rho}{\rho} g \frac{v_t}{S_c} \frac{\partial C}{\partial y}; \quad \Gamma = v_t + \nu; \quad (7a,b,c)$$

$$v_t = C_\mu \frac{k^2}{\varepsilon}$$

in which U, V = mean-flow velocity in x and y direction, respectively; θ = channel slope; P = pressure deviation from hydrostatic one; ρ = mass density of water; g = gravitational acceleration; ν = kinematic viscosity; v_t = kinematic eddy viscosity; Γ = effective viscosity; k = turbulent energy; ε = energy dissipation; P_r = production of turbulent energy due to shear stress; G = buoyant production of turbulent energy; C = particle volumetric concentration; S_c = turbulent Schmit number; and $(F_{dx}, F_{dy}), (f_{dx}, f_{dy})$ = mean and fluctuating components of drag term caused by the existence of sediment particle per unit volume.

Fluid flow around sediment particle exerts a force on the sediments, and as a consequence of the action and reaction, the same strength force, the so-called drag force, acts on the surrounding fluid of the sediment particle in the opposite direction. Hence, the interaction terms in the mean-flow equations are calculated by the spatial average of drag force for every computational grid cells. A correlation between the fluctuating drag force and the velocity fluctuation of the surrounding fluid of particle is also included in the transport equation of turbulent energy, k . The transport equation of energy dissipation, ε , is originally derived by assuming the analogy between k - and ε -equation, thus, the fluid/particle interaction term in this equation is defined similar to that of the k -equation with dimensional adjustment.

The fluctuating velocity components of the flow, u and v , is given by

$$u(t) = r_u \sqrt{u^2}; \quad v(t) = r_v \sqrt{v^2} \quad (8a,b)$$

in which r_u, r_v = random numbers following to the standard Gauss distribution in x and y directions; and $\sqrt{u^2}, \sqrt{v^2}$ = turbulent intensities in x and y directions, respectively. The two series of random numbers satisfy the two-dimensional Gauss distribution given by

$$f_r(r_u, r_v) = \frac{1}{\sqrt{2\pi}} \exp\left(-\frac{r_u^2}{2}\right) \frac{1}{\sqrt{1-\gamma^2} \sqrt{2\pi}} \cdot \exp\left\{-\frac{(r_v - \gamma \cdot r_u)^2}{2(1-\gamma^2)}\right\} \quad (9)$$

in which γ = cross-correlation coefficient of two series of the random numbers. Turbulent intensities also can be estimated based on the turbulent energy (Nezu, 1977) as follows:

$$\sqrt{u^2} = 1.108 \sqrt{k}; \quad \sqrt{v^2} = 0.036 \sqrt{k} \quad (10a,b)$$

The cross-correlation coefficient of two turbulent velocity components is related to the Reynolds stress as follows:

$$\gamma = \frac{-\overline{uv}}{\sqrt{\overline{u^2}}\sqrt{\overline{v^2}}} \quad (11)$$

The model constants are set according to Launder and Spalding (1974) as: $C_{\mu} = 0.09$, $C_{1\varepsilon} = 1.44$; $C_{2\varepsilon} = 1.92$; $C_{3\varepsilon} = 1.0$; $\sigma_k = 1.0$; $\sigma_\varepsilon = 1.3$; and $S_c = 1.0$.

2.2 Model of sediment phase

The trajectory of a saltating particle is governed by the following equations:

$$\rho\left(\frac{\sigma}{\rho} + C_M\right)A_3d^3\frac{du_p}{dt} = \frac{\rho}{2}C_D A_2d^2 \cdot \sqrt{(U + u - u_p)^2 + (V + v - v_p)^2}(U + u - u_p) \quad (12)$$

$$\rho\left(\frac{\sigma}{\rho} + C_M\right)A_3d^3\frac{dv_p}{dt} = \frac{\rho}{2}C_D A_2d^2 \cdot \sqrt{(U + u - u_p)^2 + (V + v - v_p)^2}(V + v - v_p) - \rho\left(\frac{\sigma}{\rho} - 1\right)gA_3d^3 \quad (13)$$

$$C_D = C_{D\infty} + \frac{24}{R_e}; \quad R_e = \frac{d\sqrt{(U + u - u_p)^2 + (V + v - v_p)^2}}{\nu} \quad (14)$$

in which d = diameter of sediment particle; σ = mass density of sediment; A_2 , A_3 = two- and three-dimensional geometrical coefficient of sediment; C_M = added mass coefficient; C_D = drag coefficient ($C_{D\infty} = 0.4$); and u_p , v_p = velocity component of saltating particle in x and y directions, respectively.

2.3 Boundary conditions

At the bottom, the wall function is implemented, namely the logarithmic law holds between the wall and the first grid point. Then the turbulent energy and the energy dissipation in this region are given as follows:

$$k = \frac{u_*^2}{\sqrt{C_\mu}}; \quad \varepsilon = \frac{u_*^3}{\kappa y} \quad (15a,b)$$

in which u_* = shear velocity; and κ = von-Kármán constant ($\kappa = 0.41$).

For the water surface, the symmetric boundary condition is applied in the first cycle of the calculation, then the second cycle of calculation is conducted with a modification on the turbulent energy with considering a turbulent energy damping at the water surface based on the proposal by Nezu and Nakagawa (1987).

3 Mean-flow velocity profile

3.1 Outline of experiment

The experiments were carried out in a tilting flume with a rectangular cross section, with dimensions of 9m length, 32cm depth, and 33cm width, as shown in Fig. 1 (Yeganeh, 1997). To obtain higher shear stress, the width of the working section was decreased to 12cm. The water discharge was controlled by a personal computer based on the feedback signals of an electric current meter. To implement the hydraulically rough bed condition, the bottom of channel was carefully roughened by pasting the same diameter particles as the moving sediment.

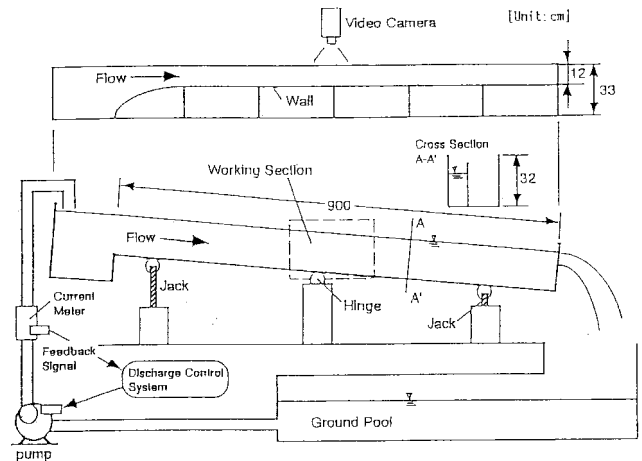


Fig. 1. Experimental flume.

The supplied sediment consisted of glass beads with 5mm diameter and a specific gravity of 2.6. The flow velocity was measured by a Pitot-tube with a 3mm outer diameter. The large size of the sediment has the merit of making possible the measurement of the flow velocity distribution even inside the intense sediment transport layer. The Pitot-tube was connected to two pressure-transducers for monitoring the dynamic and static pressure of the flow field. Analysis of pressure-transducer output was carried out by replaying the signals recorded by a digital data recorder, with the sampling rate of 50 Hz.

The flume bottom inclination began from $i_b = 0.01$, then it gradually increased up to $i_b = 0.05$. In the case of the bottom inclination $i_b = 0.03$, sediment particles were transported in the pure saltation mode. Then transition from the saltation to the hyper-concentrated mode has been observed with the increase of the bottom inclination. Finally, at the bottom inclination $i_b = 0.05$, hyper-concentrated sediment transport with frequent interparticle collision was reproduced. The experimental conditions are shown in Table 1.

Table 1. Experimental hydraulic condition.

i_b	$h(\text{cm})$	$U_m(\text{cm/s})$	$u_*(\text{cm/s})$	τ_*	$q_w(\text{cm}^2/\text{s})$	$q_s(\text{cm}^2/\text{s})$
0.03	3.85	108.2	10.86	0.146	420	5.21
0.03	4.76	131.3	12.49	0.193	620	6.41
0.03	5.70	146.2	13.10	0.212	833	8.33
0.05	3.20	130.2	13.03	0.210	420	8.33
0.05	4.23	147.75	14.69	0.267	620	10.42
0.05	5.04	165.3	16.50	0.337	833	16.90

3.2 Characteristics of mean-flow velocity profile

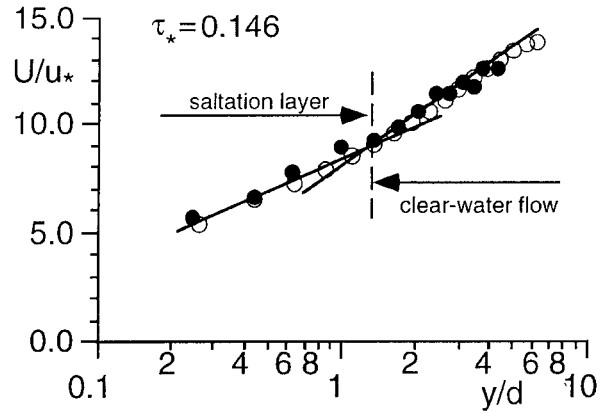
Fig. 2 depicts the simulation result of the mean-velocity profile in comparison with that of the experimental one (Yeganeh, 1997), at moderate flow intensity with the flume bottom inclination $i_b = 0.03$. The simulation result shows a very good agreement with the experiment. The figure shows that the mean velocity tends to a two-layer type profile with different velocity gradient in each layer. The milder gradient part of the profile coincides with the saltation layer, while at a certain transition point it changes to the steeper gradient approximately $1/\kappa$ in the clear-water flow. This kind of profile was reproduced numerically by Gotoh et al. (1994) by the two-phase flow model with the PSI-cell concept for the fluid/particle interaction.

The way in which the mean velocity of the sediment-laden flow varies with the bottom shear stress is studied experimentally by Yeganeh (1997). He reveals that the two-layer type profile is the characteristics of the mean velocity under the moderate flow intensity with rather low rate of the sediment transport in the saltation mode. According to Gotoh et al. (1994), the mechanism of two-layer type profile can be interpreted as follows. In the saltation layer, there are two paths of the vertical momentum transfer: (i) the momentum transfer due to the vertical mixing of the fluid; and (ii) that due to the vertical motion of the sediment particles keeping interaction with surrounding fluid. An additional momentum transport due to saltation causes a significant increase in the vertical momentum transfer of the fluid-sediment mixture. Therefore, the velocity profile has a milder slope in this region. It is evident that the fluid/particle interaction is the predominant hydrodynamic mechanism of the bed-load transport at moderate flow intensity.

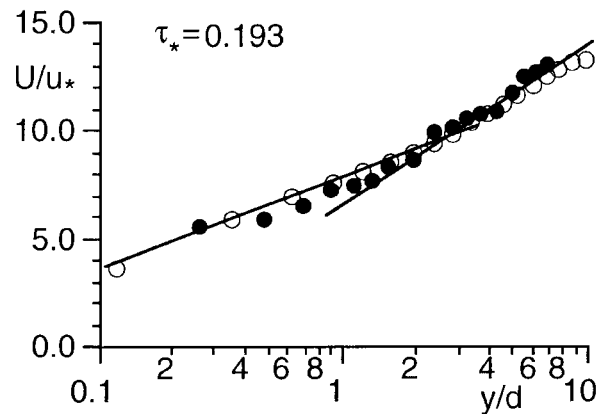
With the increase of the flow intensity, a hyper-concentrated layer of the moving sediments takes place in the bottom neighborhood. In this layer, the moving sediments collide to each other very frequently, hence the so-called particle/particle interaction becomes the predominant mechanism. Since the interparticle collision dissipates the fluid energy in a very high rate, and damps the bottom generated fluid turbulence, it brings significant change into the mean-flow velocity profile.

Fig. 3 gives a comparison between the measured mean-flow velocity and the simulation result under the three different flow intensity in the cases of $i_b = 0.05$. Even though the particle/particle interaction is not considered in the simulation model, the fairly good agreement between the experiment and the simulation is found in the upper region of velocity profile. In the bottom region, however,

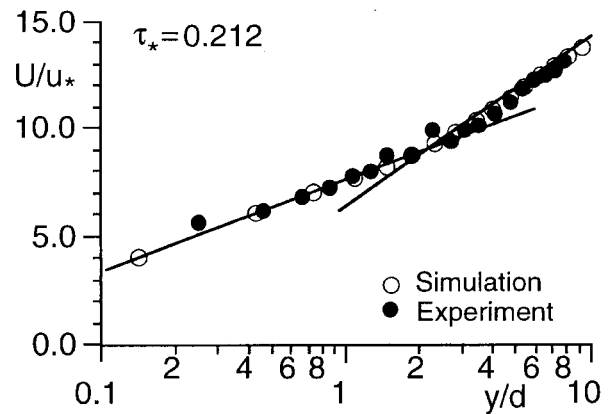
a clear discrepancy can be observed between the simulation and the experiment. The experimental velocity profile shows upward concave form, which may follow a power-law distribution proposed by Sumer, Kozakiewicz, Fredsøe and Deigaard (1996), whereas the velocity profile of the simulation is upward convex one. This would apparently leads to the existence of the different governing mechanism of the velocity profile in the hyper-concentrated layer between the simulation and the experiment, which is not taken into account in the present simulation.



(a) $Q=5.0 (10^3 \text{ cm}^3/\text{s})$

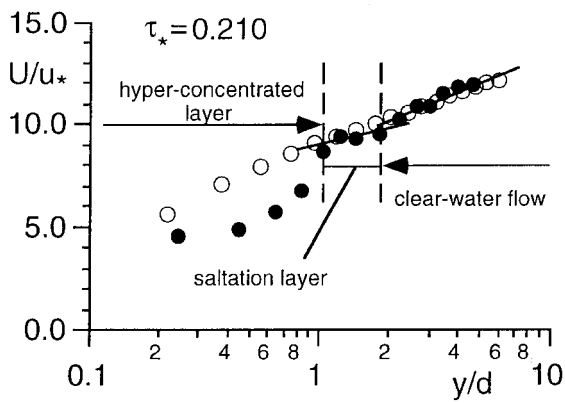


(b) $Q=7.5 (10^3 \text{ cm}^3/\text{s})$

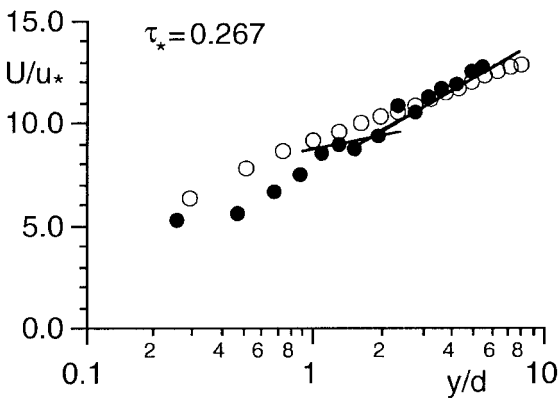


(c) $Q=10.0 (10^3 \text{ cm}^3/\text{s})$

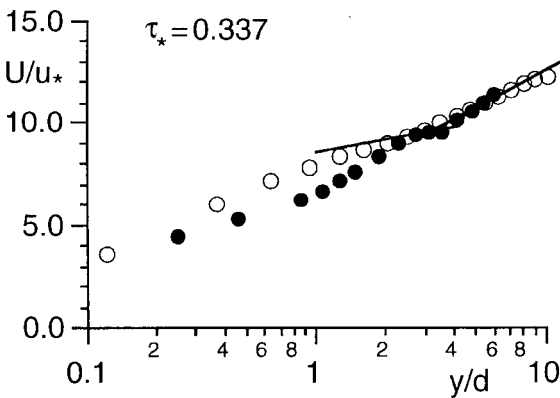
Fig. 2. Two-layer type velocity profile.



(a) $Q=5.0 (10^3 \text{ cm}^3/\text{s})$



(b) $Q=7.5 (10^3 \text{ cm}^3/\text{s})$



(c) $Q=10.0 (10^3 \text{ cm}^3/\text{s})$

Fig. 3. Three-layer type velocity profile.

4 Structure of mean-flow velocity field

Fig. 4 presents the Reynolds stress distribution of the simulated result for the moderate flow intensity in the cases of $i_b = 0.03$, and that for the high flow intensity in the cases of $i_b = 0.05$. In general, the Reynolds stress declines from the triangle distribution, which is an indication of the clear-water region, as the effect of the moving sediments becomes significant. The elevation at which it departs from the triangle distribution is shifting upward in the cases of high flow intensity, or $i_b = 0.05$. It means that the effect of the moving sediment spreads in a wider range

in the case of $i_b = 0.05$ than the case of $i_b = 0.03$. The decreasing rate of the Reynolds stress is associated with the provided momentum from the flow phase to the sediment one to maintain the saltation motion.

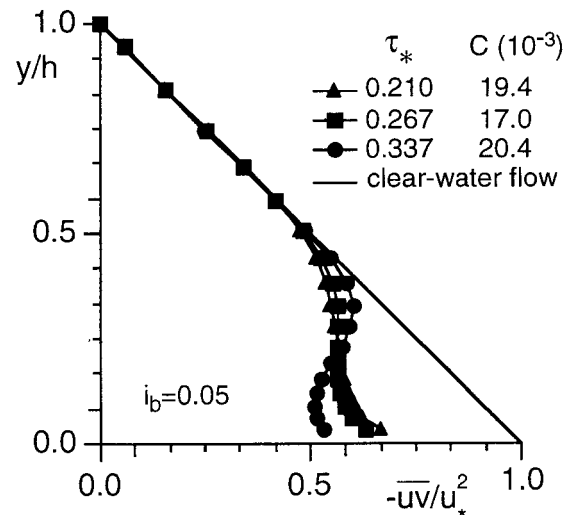
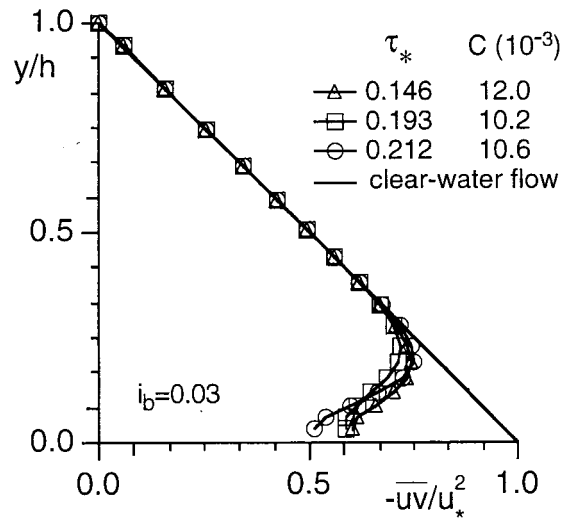


Fig. 4. Reynolds stress distribution.

Fig. 5 shows the distributions of the kinematic eddy viscosity simulated by the present model for the various cases of the flow intensities. At the bottom neighboring region, in which the sediment is transported, an approximately linear distribution can be observed. The region of the linear distribution becomes large with the increase of the flume inclination, which brings the increase of the height of saltation. As a result of the turbulent energy damping at the water surface in the model, the kinematic eddy viscosity commonly decreases toward the water surface after having its peak in the middle of the flow depth. In the case of $i_b = 0.05$, the kinematic eddy viscosity shows the significant difference for the different bottom shear stress; while, in the case of $i_b = 0.03$, the kinematic eddy viscosity does not respond keenly to the change of the bottom shear stress.

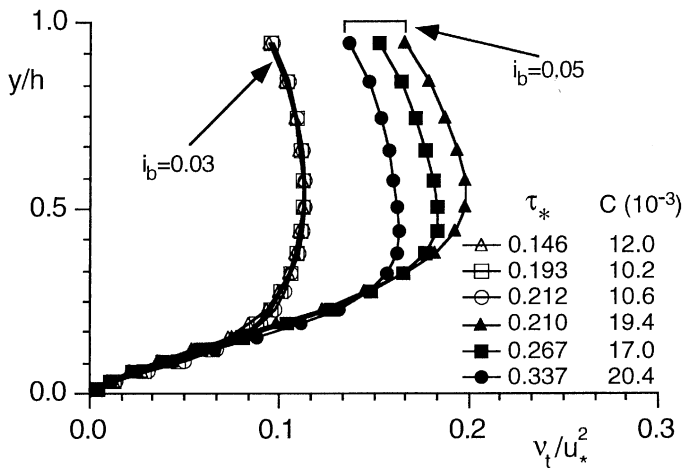


Fig. 5. Kinematic eddy viscosity distribution.

Fig. 6 presents the distribution of the turbulent energy. It is also seen that the higher flow intensity in the cases of $i_b = 0.05$ causes higher rate of turbulent energy than that of the moderate flow intensity in the cases of $i_b = 0.03$. The difference of the distribution for the change of the bottom shear is more clear in the cases of $i_b = 0.05$ than the cases of $i_b = 0.03$.

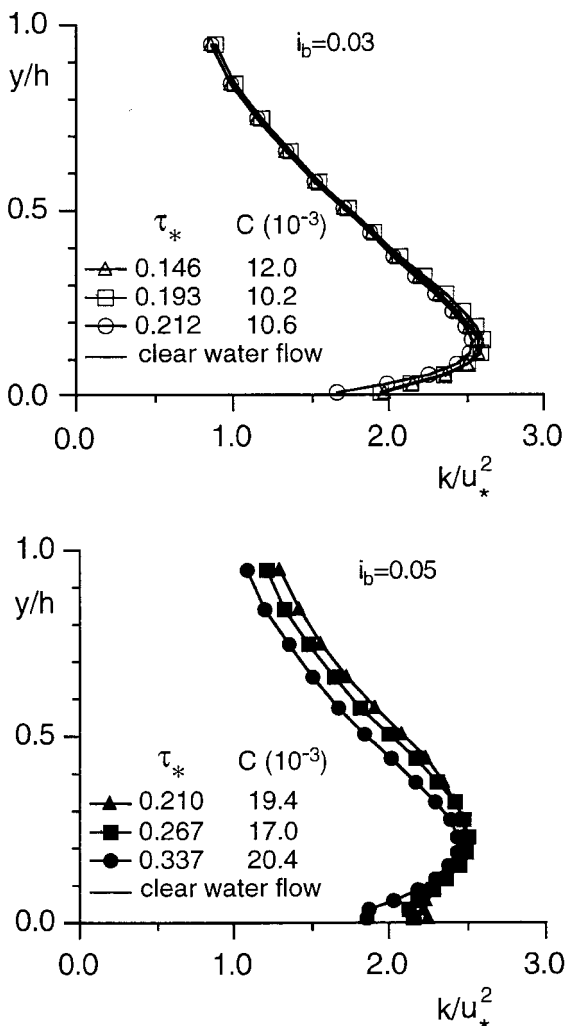


Fig. 6. Turbulent energy distribution.

The mean velocity profile is determined as the result of the momentum transfer due to the turbulence. Hence the characteristics of the mean velocity profile, or the existence of the two-layer and three-layer velocity profiles aforementioned, can be explained based on the distributions of the properties of turbulence. In steady and uniform flow, the mean-flow velocity can be related to the Reynolds stress and the kinematic eddy viscosity as follows:

$$\frac{\partial U}{\partial y} = \frac{1}{\nu_t}(-\overline{uv}) \quad (16)$$

By differentiating the logarithmic velocity profile, the velocity gradient can be written in the following form.

$$\frac{\partial U}{\partial y} = \frac{u_*}{\kappa y} \quad (17)$$

Consequently, when the mean velocity follows the logarithmic profile, the ratio of the Reynolds stress to the kinematic eddy viscosity is inversely proportional to y -coordinates as follows:

$$1 = \frac{\kappa d}{u_*} \cdot \left(\frac{-\overline{uv}}{\nu_t} \right) \cdot \left(\frac{y}{d} \right) \quad (18)$$

In the clear-water layer, this relation should be satisfied. While, in the saltation layer, in which the simulation data shows logarithmic velocity profile with a different gradient from that for the clear-water flow, Eq. 18 also can be applicable by changing the proportional factor, or Kármán constant. Fig. 7 shows this relation for the cases of $i_b = 0.03$ and $i_b = 0.05$. Two straight lines mean Eq. 18, which satisfies the logarithmic velocity profile for the different Kármán constants, $\kappa = 0.41$ and 0.3 . In the case of $i_b = 0.03$, the simulation results, which agree with the straight line of $\kappa = 0.41$ in the upper layer, shift downward in the middle range, or $1.0 < y/d < 3.0$. In the lower part of the flow, the simulation results agree with the straight line of $\kappa = 0.3$. This fact shows that the turbulent structure also supports the existence of the two-layer type profile in the mean-flow velocity. While, in the case of $i_b = 0.05$, the simulation results, which follow the straight line of $\kappa = 0.41$ in the upper layer, shift downward in the middle range, or $2.0 < y/d < 4.0$. The simulation results, which follow the line of $\kappa = 0.3$ in a certain region, shift upward again from the line of $\kappa = 0.3$ with going downward. This fact roughly agrees with the tendency of the gradient of the velocity profile in Fig. 3, which becomes once milder in the middle and becomes steeper in the lower part. In Fig. 3, the experimental results shift from the straight line of the middle part with following the upward concave curves; while, the results of the present simulation cannot reproduce such drastic change of the velocity gradient. The results of the simulation, in which the solid phase is modeled as the ensemble of the mutually independent saltations, show the gradual increase of the gradient of the velocity profile.

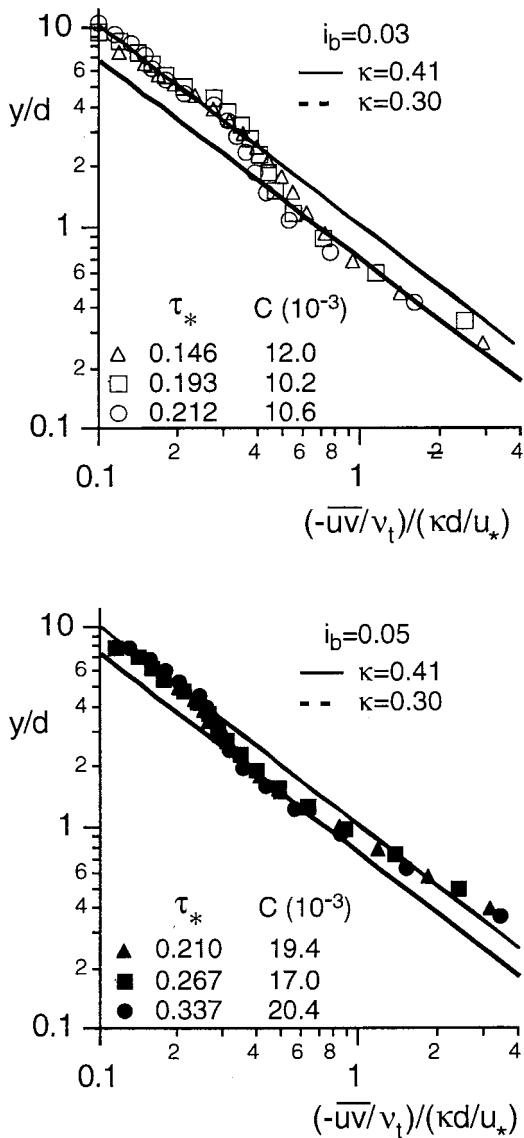


Fig. 7. Characteristics of Kármán constant.

5 Characteristics of sediment motion

5.1 Results of present simulation

Fig. 8 shows the distribution of the streamwise mean velocity of moving particles of the simulation, or u_p , normalized by the bulk mean-flow velocity, or U_m . For the cases under the same condition of the channel slope, the parameter U_m is an appropriate factor to normalize the velocity of moving particle. On the other hand, the velocity of moving particle show the clear difference between two different channel slope, or $i_b = 0.03$ and 0.05 .

The existing-probability-density of the saltating particles are presented in Fig. 9. It can be observed that the peak of the existing-probability-density shifts upward with the increases of the bottom shear stress. Because the higher flow intensity provides the higher rate of momentum for the saltating particles, the existing-probability of the saltating particles at a higher elevation increases with the increase of the flow intensity. There are common trends in the existing-probability-density distributions: it increases in the bottom neighboring region, and it decreases

in upward direction after having a peak at a certain elevation. The clear difference in the thickness of the existing-probability-density increasing region can be detected between two different channel slopes, or $i_b = 0.03$ and 0.05 .

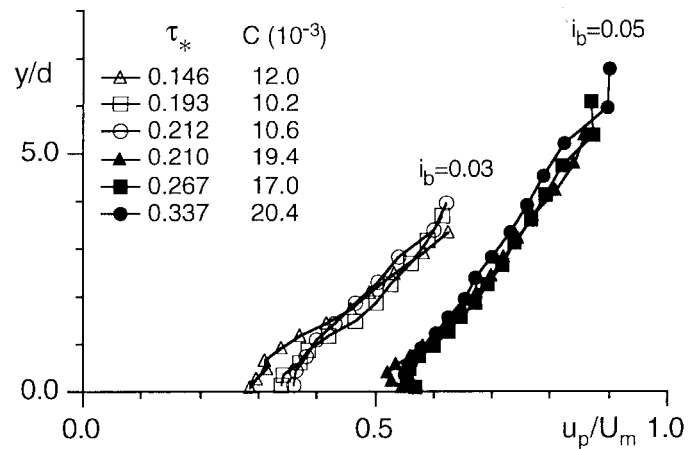


Fig. 8. Velocity profile of particles.

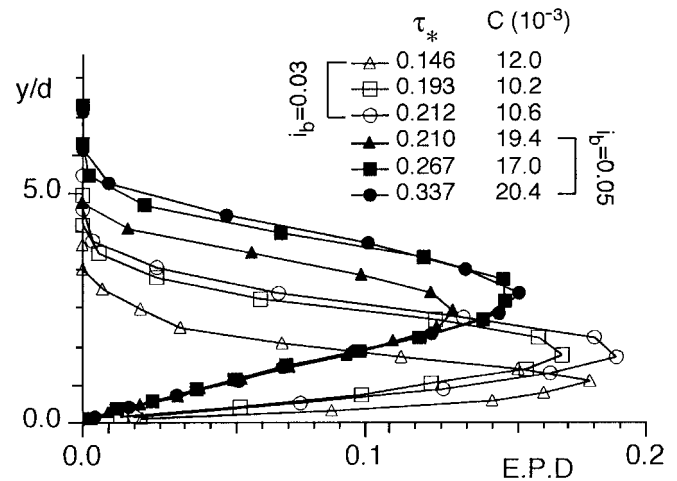


Fig. 9. Existing-probability-density of particles.

Fig. 10 shows the probability-density profile of the collision- and repulsion-angle of the moving practices, θ_{in} and θ_{out} , at the different bottom shear stress, τ_* . Based on these kinds of information of the statistical characteristics of the sediment motion, the detail behavior of the saltation under the different level of the bottom shear can be estimated. In the case of $i_b = 0.05$, the probability-density of the collision angle, θ_{in} , distributes in a very narrow range, namely 10-20 degree, while in the case of $i_b = 0.03$, the probability-density of θ_{in} distributes in approximately twice wider range than that of $i_b = 0.05$. In the case of $i_b = 0.05$, the distribution of probability-density is roughly symmetric; while, in the case of $i_b = 0.03$, it shows the clear asymmetry. As for both of the two cases, or $i_b = 0.03$ and 0.05 , the repulsion angle distributes in a wide range. In detail, the probability-density in the case of $i_b = 0.03$ shows a weak increasing tendency with the repulsion angle, while it increases clearly in the case of $i_b = 0.05$. Roughly speaking, the saltation in the cases of $i_b = 0.05$ collides with the bottom in smaller angle, and it repulses in a larger angle in comparison with the saltation in the case of $i_b = 0.03$.

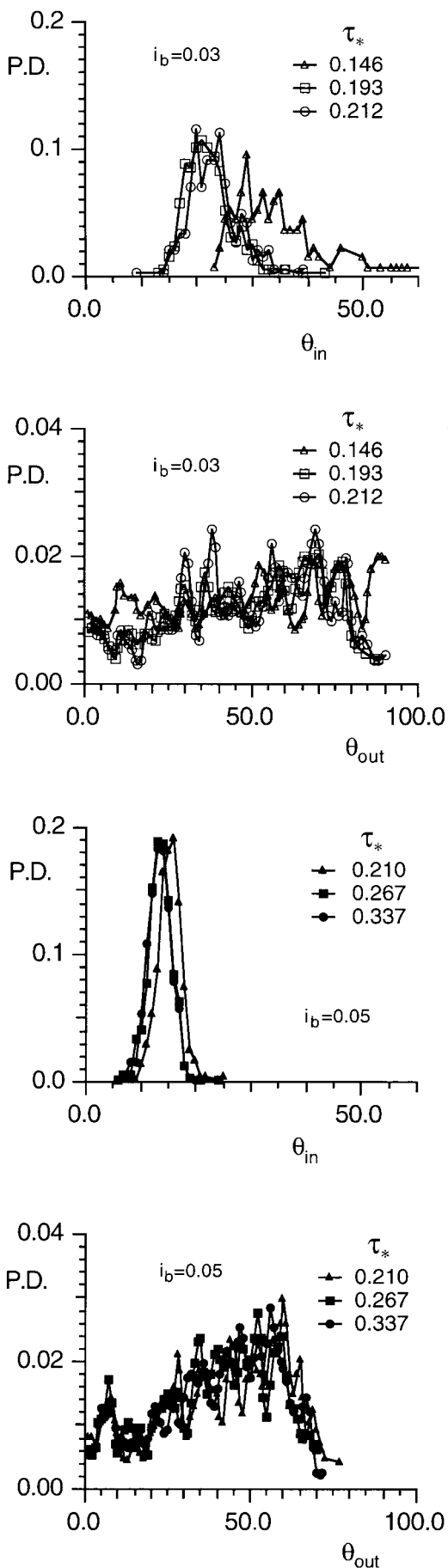


Fig. 10. Collision- and repulsion-angle distribution.

The average as well as the maximum height of the saltating particles, H_{av} and H_{max} , normalized by the particle diameter and the water depth versus non-dimensional bottom shear stress, τ_* , are depicted in Fig. 11. Needless to say, both of the absolute value of the average and maximum height of saltation increase with the bottom shear stress, while the increasing rate of the saltation height becomes weak in the case of $i_b = 0.05$. The relative height of the saltation to the water depth tends to decrease in the case of $i_b = 0.05$.

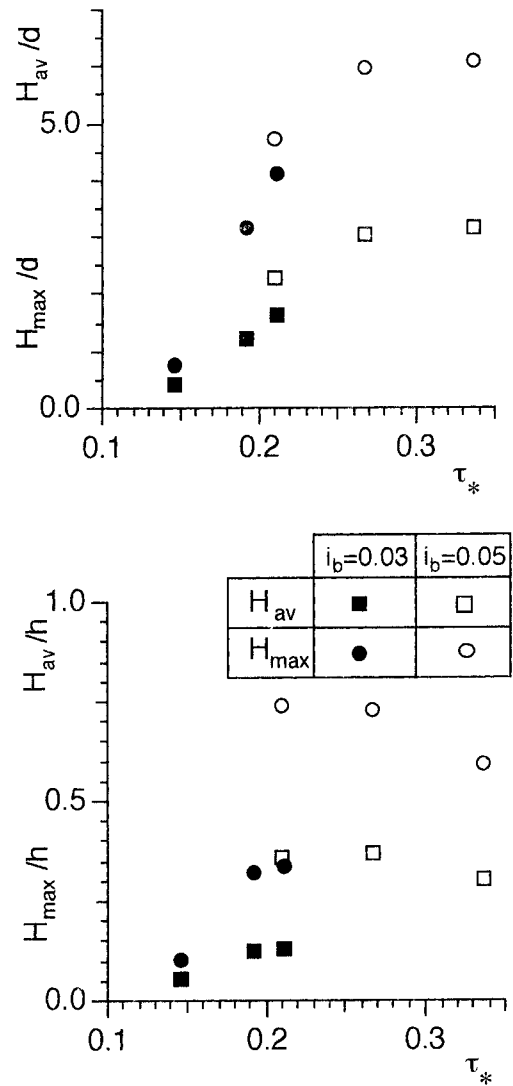


Fig. 11. Height of saltation.

5.2 Limitation of applicability of saltation model

The calculated results in the cases of $i_b = 0.05$ indicates the limitation of the applicability of saltation model, or the single particle tracing model, under the action of high bottom shear. The velocity profile in Fig. 8 shows the monotonously increasing behavior similar to that of $i_b = 0.03$. In the proximity of the bottom, the effect of the interparticle collision is more predominant in the case of $i_b = 0.05$ than that of $i_b = 0.03$, hence there should be some indications of the decrease of particle velocity. The existing-probability-density distribution in Fig. 9 calculated by the saltation model has a peak, in other words, there is the decreasing range of the existing-probability-density. This

decreasing range of the existing-probability-density of $i_b = 0.05$ is approximately four times thicker than that of $i_b = 0.03$. Under the action of the high bottom shear, the sheetflow layer with highly concentrated sediments are usually formed in the proximity of the bottom. This type of behavior of particles is observed in the experiment. The saltation model cannot reproduce this characteristic, because it cannot simulate the interparticle collision. The relative height of the saltation in Fig. 11 calculated by the saltation model tends to decrease in the case of $i_b = 0.05$ in spite of the increase of bottom shear stress. In saltation model, the momentum transport due to the motion of sediment is taken by the single large scale saltation in the case of $i_b = 0.05$. Although the momentum is actually transferred in vertical direction one by one through the interparticle collisions, the saltation model cannot reproduce this characteristic. All of these facts indicates the difficulty in applying the saltation model in the case of $i_b = 0.05$.

6 Conclusive remarks

The three-layer structure of the flow velocity profile, which was found in the experiment under the high bottom shear, cannot be reproduced by the saltation model. The application of the saltation model is contrary to the actual behavior of the sediment particles under the high bottom shear. Although the existence of the sheetflow layer, in which the interparticle collision is the predominant mechanism of the momentum transport is clarified in the experiment, the saltation model, or the single particle tracing model, cannot express this type of sediment motion. The model, which can reproduce the effect of the interparticle collision, is required to be coupled with the model of the flow/sediment interaction treated in the present study, to enlarge the applicable range of the framework of the present model. The authors have already performed the numerical simulation of the granular materials based on the Distinct Element Method (Gotoh and Sakai, 1997). The appendix shows how to modify the author's granular material model to be coupled with the k - ϵ flow-turbulence model presented herein. By coupling the model of flow-sediment interaction and the granular material model, the difficulty of the present model under the high bottom shear will be resolved.

Acknowledgement

The authors wish to express their gratitude to Dr. T. Asano, Assoc. Prof. at Kagoshima Univ., for his very useful comments, and also are grateful to Prof. I. Nezu and his laboratory staffs at Kyoto Univ., for their help in conducting the experiments.

Appendix: Coupling with granular material model

The sediment particles are modeled by the rigid cylinders with an uniform diameter. Among each cylinder, the spring and dashpot systems are introduced to express the particle/particle interaction. Equations of motion of the individual particle are solved by the explicit method in the vertically two-dimensional plane (see Gotoh and Sakai, 1997).

Equations of motion of particle, or Eqs. 12 and 13, can be modified with taking the particle/particle interaction forces into account. Then the equations of motion of the i -th particle are as follows:

$$\rho \left(\frac{\sigma}{\rho} + C_M \right) A_3 d^3 \frac{du_{pi}}{dt} = \sum_j \{ -f_n \cos \alpha_{ij} + f_s \sin \alpha_{ij} \}_j + \frac{1}{2} \rho C_D \sqrt{(U + u - u_{pi})^2 + (V + v - v_{pi})^2} (U + u - u_{pi})^2 A_2 d^2 \quad (A1)$$

$$\rho \left(\frac{\sigma}{\rho} + C_M \right) A_3 d^3 \frac{dv_{pi}}{dt} = \sum_j \{ -f_n \cos \alpha_{ij} + f_s \cos \alpha_{ij} \}_j + \frac{1}{2} \rho C_D \sqrt{(U + u - u_{pi})^2 + (V + v - v_{pi})^2} (V + v - v_{pi}) A_2 d^2 - \rho \left(\frac{\sigma}{\rho} - 1 \right) A_3 d^3 g \quad (A2)$$

$$\frac{\pi d^5}{32} \frac{d\omega_{pi}}{dt} = \frac{d}{2} \cdot \sum_j \{ f_s \}_j \quad (A3)$$

in which u_{pi} , v_{pi} = velocity of particles in the streamwise and upward-vertical directions; f_n , f_s = normal and tangential components of the force acting on the contacting plane between the i -th and j -th particles on the local coordinate system; α_{ij} = contacting angle between the i -th and j -th particles; and ω_{pi} = angular velocity of the i -th particle. These sets of the equation of motion are solved explicitly to trace the motion of the individual particles. In these sets of equations, the rotational motion of particles due to the frictional force acting on the surface of particles are also considered. In the original code of Gotoh and Sakai (1997), the flow-sediment interaction term was written in a very simple form, in which the total bottom shear stress are distributed to the individual sediment particles directly. While, in these sets of equations, the flow-sediment interaction terms are described as the drag force term, which is appropriate form to take the local flow structure into consideration.

With rewriting the subroutines of the flow-sediment interaction in Gotoh and Sakai's numerical code, the velocity profile of sediment particles and the number-density-distribution of particles are calculated under the given flow velocity profile following logarithmic law. Figures 12 and 13 show the velocity profile of sediment particles and the number-density-distribution of particles, respectively. The velocity of particle shows the upwardly convex profile in the region $y/d < 0.0$; however, in the region $y/d > 0.0$, it shows the upwardly concave profile. Hence the inflection point exists in the proximity of $y/d = 0.0$. There exist a non-zero region of the velocity of particle beneath the elevation, at which the flow velocity becomes zero. This non-zero velocity region means the existence of the fluid-sediment mixture layer around the initial surface of the sediment depositing layer. The number-density profile shows the high level of the concentration of sediment in this layer, where the significant effect of the existence of the sediment particle on the flow structure is expected. These facts indicate the significant change of the flow velocity

profile in the neighborhood of the bottom surface by coupling the granular material model with the present model of flow.

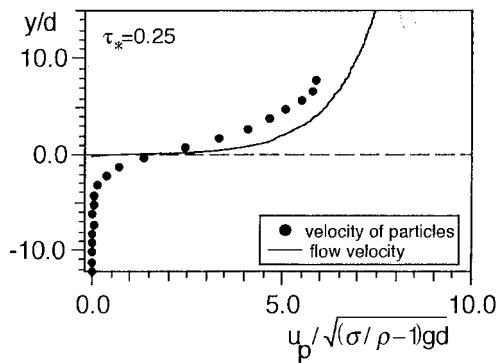


Fig. 12. Velocity profile of sediment particles.

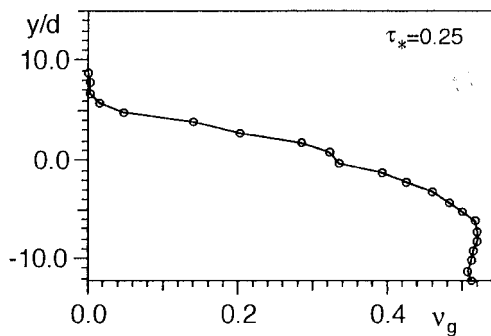


Fig. 13. Number-density-distribution of particles.

References

- ASANO, T. (1990): Two-phase flow model on oscillatory sheet-flow, *Proc., 22nd ICCE, Delft, Netherland*, pp. 2372-2384.
- BAKKER, W. T. and VAN KESTEREN, W. G. M. (1986): The dynamics of oscillatory sheetflow, *Proc., 20th, ICCE, Taipei, Taiwan*, pp. 940-954.
- GOTOH, H., TSUJIMOTO, T. and NAKAGAWA, H. (1994): Numerical model of interphase momentum transfer and interparticle collision in bed-load layer, *Proc., APD-IAHR*, pp. 565-572.
- GOTOH, H. and SAKAI, T. (1997): Numerical simulation of sheetflow as granular materials, *J. Waterway, Port, Coastal and Ocean Eng., ASCE*, Vol. 123, No. 6, pp. 329-336.
- KOBAYASHI, N. and SEO, S. N. (1985): Fluid and sediment interaction over a plan bed, *J. Hydr. Engrg., ASCE*, 111(6), pp. 903-921.
- LAUNDER, B. E. and SPALDING, D. B. (1974): The numerical computation of turbulent flow, *J. Comp. Meth. in Appl. Mech. and Engrg.*, No. 3, pp. 269-289.
- NEZU, I. (1977): Turbulent structure in open-channel flows, *Ph.D. Thesis, Kyoto university*. (in Japanese)
- NEZU, I. and NAKAGAWA, H. (1987): Numerical calculation of turbulent open-channel flows in consideration of free-surface effects, *Mem. Fac. Eng., Kyoto Univ.*, Vol. 49, No. 2, pp. 111-145.
- SHIELDS, A. (1936): Anwendung der Aehnlichkeitsmechanik und Turbulenzforschung auf die Geschiebepbewegung, *Mitt Preuss Versuchsanstalt fur Wasserbau und Schiffbau*, No. 26, Berlin.
- SUMER, B.M., KOZAKIEWICZ, A., FREDSE, J. and DEIGAARD, R. (1996): Sheet-flow measurements in steady currents, *J. Hydr. Engrg., ASCE*, Vol. 122, No. 10, pp. 549-558.
- WIBERG, P. L. and SMITH, J. D. (1989): Model for calculating bed-load transport of sediment, *J. Hydr. Engrg., ASCE*, 115(1), pp. 101-123.
- YEGANEH, A. (1997): Velocity profile of sediment-laden flow in transition from saltation to sheet-flow, *Proc. XXVII IAHR Cong., San Francisco, USA, JFK- SP*, pp. 1-6.

Notations

- A_2, A_3 two- and three-dimensional geometrical coefficient of sediment;
- C particle volumetric concentration;
- C_D drag coefficient;
- C_M added mass coefficient;
- C_w, C_{ie} constants in $k-\epsilon$ model ($i = 1, 2, 3$);
- d diameter of saltating particle;
- F_{dx}, F_{dy} mean value components of the fluid/particle interaction term per unit volume;
- f_{dx}, f_{dy} fluctuating components of the fluid/particle interaction term per unit volume;
- f_n, f_s normal and tangential components of the force acting on the contacting plane between the i -th and j -th particles on the local coordinate system;
- G buoyant production of turbulent energy;
- g gravitational acceleration;
- H_{av}, H_{max} average and maximum height of saltating particles;
- h flow depth;
- i_b channel bottom inclination;
- k turbulent energy;
- P pressure deviation from hydrostatic one;
- P_r production of turbulent energy due to shear stress;
- r_u, r_v random numbers following to the standard Gauss distribution in x, y directions;
- S_c turbulent Schmit number;
- U, V mean-flow velocity in x, y direction, respectively;
- U_m bulk mean-flow velocity;
- u, v instantaneous flow velocity in x, y direction, respectively;
- $\sqrt{\overline{u^2}}, \sqrt{\overline{v^2}}$ turbulent intensities in x and y directions, respectively;
- u_p, v_p velocity component of saltating particle in x, y directions;
- u_{pi}, v_{pi} velocity of particles in the streamwise and upward-vertical directions;
- $-\overline{uv}$ Reynolds stress;
- u_* shear velocity;
- x, y streamwise and upward vertical coordinates;
- α_{ij} contacting angle between the i -th and j -th particles;
- Γ effective viscosity;
- γ cross-correlation coefficient of two series of the random numbers in Monte-Carlo simulation;
- ϵ energy dissipation;
- θ channel slope;
- θ_m, θ_{out} the mean collision and repulsion angle;
- κ von-Kármán constant ($= 0.41$);
- ν kinematic viscosity;
- ν_t kinematic eddy viscosity;
- ρ mass density of water
- σ mass density of sediment;
- $\sigma_k, \sigma_\epsilon$ constants in $k-\epsilon$ model;
- τ_* non-dimensional bottom shear stress; and
- ω_{pi} angular velocity of the i -th particle.